

~~RESTRICTED~~

UNCLASSIFIED

Copy

6

RM A50H23

N-2179

C12



# RESEARCH MEMORANDUM

WIND-TUNNEL INVESTIGATION OF THE EFFECTS OF  
A JET-ENGINE NACELLE ON THE AERODYNAMIC  
CHARACTERISTICS OF A  $37.25^\circ$  SWEPT-BACK  
WING AT HIGH SUBSONIC SPEEDS

By Frederick W. Boltz and Donald A. Buell

Ames Aeronautical Laboratory  
Moffett Field, Calif.

CLASSIFICATION CANCELLED

Authority J. W. Crowley Date 2/11/53

EO 10501

By MAA 1/8/54 See NACA

CLASSIFIED DOCUMENT R 7-1877

This document contains classified information affecting the National Defense of the United States within the meaning of the Espionage Act, USC 50:31 and 32. Its transmission or the revelation of its contents in any manner to an unauthorized person is prohibited by law.

Information so classified may be imparted only to persons in the military and naval services of the United States, appropriate civilian officers and employees of the Federal Government who have a legitimate interest therein, and to United States citizens of known loyalty and discretion who of necessity must be informed thereof.

## NATIONAL ADVISORY COMMITTEE FOR AERONAUTICS

WASHINGTON  
October 24, 1950

~~RESTRICTED~~

UNCLASSIFIED



UNCLASSIFIED

## NATIONAL ADVISORY COMMITTEE FOR AERONAUTICS

RESEARCH MEMORANDUMWIND-TUNNEL INVESTIGATION OF THE EFFECTS OF A JET-ENGINE NACELLE  
ON THE AERODYNAMIC CHARACTERISTICS OF A  $37.25^\circ$ 

## SWEPT-BACK WING AT HIGH SUBSONIC SPEEDS

By Frederick W. Boltz and Donald A. Buell

## SUMMARY

A wind-tunnel investigation has been made to determine the aerodynamic characteristics of a wing-nacelle combination at high subsonic speeds. The model consisted of a jet-engine nacelle in combination with a wing having the leading edge swept back  $37.25^\circ$  and having an aspect ratio of 6.04. The nacelle was mounted on the lower surface of the wing with the air inlet slightly behind the wing leading edge and normal to the nacelle axis.

Lift, drag, pitching-moment, and ram-recovery data are presented for the wing-nacelle combination for Mach numbers from 0.18 to 0.92 at a constant Reynolds number of 2,000,000. Surface pressure data are presented for Mach numbers near that of drag divergence.

The addition of the nacelle to the wing was found to have little effect on the lift and pitching-moment characteristics of the wing. At lift coefficients between -0.1 and 0.4, the drag-divergence Mach number of the wing-nacelle combination was about 0.01 or less lower in value than that of the wing alone. The reduction of flow through the nacelle to zero slightly increased the drag at Mach numbers below that of drag divergence, but had little effect on the Mach number of drag divergence.

At moderate positive angles of attack, the ram-recovery ratio at a station 4 percent of the nacelle length behind the nacelle inlet increased from approximately 0.97 at a Mach number of 0.18 to approximately 0.99 at a Mach number of 0.92. The inlet-velocity ratios corresponding to these ram-recovery ratios were 0.9 and 0.6, respectively.

UNCLASSIFIED

## INTRODUCTION

The effects of a nacelle on the aerodynamic characteristics of a swept-back wing have been the subject of a series of tests at the Ames Laboratory. Investigations were made of various wing-nacelle combinations in which the wing had a leading-edge sweepback of  $37.25^\circ$  and an aspect ratio of 6.04.

In the initial phase of the program, low-speed tests as reported in reference 1 were directed at finding the most favorable position on the wing for mounting a nacelle represented by a solid ellipsoidal body. The position selected on the basis of low interference velocities in the junctures was that with the nose of the nacelle near the leading edge of the wing. Further low-speed tests, reported in reference 2, were conducted on nacelles mounted in this position to determine a satisfactory inlet shape for a jet-engine nacelle with internal flow. The best ram-recovery characteristics were obtained with the air inlet normal to the air stream and with the nacelle mounted on the lower surface of the wing at an inboard station.

The second phase of the program consisted of tests up to high subsonic Mach numbers. Results of tests of the wing alone were presented in reference 3. A body of revolution, similar to the ellipsoidal body used in the low-speed tests but having a more streamlined afterbody shape, was tested both alone and mounted at an inboard station on the lower surface of the wing. The results of these tests were reported in reference 4.

In the investigation of the present report, the wing-nacelle combination determined to be most promising from the data of reference 2 was tested in the Ames 12-foot pressure wind tunnel up to high subsonic speeds. The nacelle was mounted on the lower surface of the wing at the 31-percent-semispan station with the air inlet slightly behind the wing leading edge and normal to the nacelle axis. Internal-flow characteristics are presented along with the force, moment, and surface pressure data.

## NOTATION

$C_D$	external drag coefficient $\left( \frac{\text{external drag}}{q_0 S} \right)$
$\Delta C_D$	incremental drag coefficient $\left( \frac{\text{external drag due to addition of the nacelle}}{q_0 S} \right)$
$C_L$	lift coefficient $\left( \frac{\text{lift}}{q_0 S} \right)$

- $C_m$  pitching-moment coefficient about the quarter point of the mean aerodynamic chord  $\left( \frac{\text{pitching moment}}{q_o S \bar{c}} \right)$
- $H$  arithmetic average of the total pressure at a given station in nacelle duct, pounds per square foot
- $H_o$  free-stream total pressure, pounds per square foot
- $\frac{H - p_o}{H_o - p_o}$  ram-recovery ratio
- $L/D$  lift-to-drag ratio
- $M_D$  drag-divergence Mach number  $\left[ \begin{array}{l} \text{the free-stream Mach number at} \\ \text{which} \left( \frac{\partial C_D}{\partial M_o} \right)_{C_L} = 0.10 \end{array} \right]$
- $M_o$  free-stream Mach number
- $P$  local pressure coefficient  $\left( \frac{p - p_o}{q_o} \right)$
- $R$  Reynolds number  $\left( \frac{\rho_o V_o \bar{c}}{\mu} \right)$
- $S$  semispan wing area, square feet
- $V_1$  average velocity at the station of minimum nacelle-inlet area, feet per second
- $V_o$  free-stream velocity, feet per second
- $V_1/V_o$  inlet-velocity ratio
- $b/2$  wing semispan, measured normal to the plane of symmetry, feet
- $c$  local wing chord, measured parallel to the plane of symmetry, feet
- $\bar{c}$  mean aerodynamic chord  $\left( \frac{\int_0^{b/2} c^2 dy}{\int_0^{b/2} c dy} \right)$ , feet
- $p$  local static pressure, pounds per square foot
- $p_o$  free-stream static pressure, pounds per square foot
- $q_o$  free-stream dynamic pressure  $\left( \frac{1}{2} \rho_o V_o^2 \right)$ , pounds per square foot
- $y$  perpendicular distance from the plane of symmetry to a point on the wing, feet

$\alpha$	angle of attack, degrees
$\alpha_u$	uncorrected angle of attack, degrees
$\mu$	coefficient of viscosity, slugs per foot-second
$\rho_0$	free-stream mass density, slugs per cubic foot

### MODEL AND APPARATUS

The model wing had a leading-edge sweepback of  $37.25^\circ$ , an aspect ratio of 6.04, a taper ratio of 0.5, no geometric twist, and the NACA 641-212 section normal to the quarter-chord line. A sketch of the plan form of the wing-nacelle combination is shown in figure 1. The model nacelle was a 1/6-scale representation of a nacelle designed to house a jet engine having a diameter of 39 inches. The nacelle nose and forebody had a shape approximately that of the NACA 1-series nose inlet. Complete design details are given in reference 2, and a control line drawing adapted therefrom is presented in figure 2 of this report.

The nacelle was mounted on the lower surface of the wing at the 31-percent-semispan station with the plane of the nacelle inlet normal to the nacelle axis and 10 percent of the chord behind the wing leading edge. For the condition of zero inlet velocity a faired tail plug, as shown dotted in figure 1, was used to stop the flow of air through the nacelle duct.

Chordwise rows of pressure orifices were located on the upper and lower surfaces of the wing at the four spanwise stations indicated in figure 1 and also along the 40-percent-chord line at approximately 4-inch intervals. In addition, pressure orifices were located in the wing-nacelle junctures, along the upper and lower nacelle meridians, and over the lip of the inlet.

The model was mounted in the wind tunnel as shown in figure 3 with the floor of the tunnel serving as a reflection plane. The balance system was connected directly to the turntable upon which the model was mounted. Pressures were measured by means of multiple-tube manometers, the readings of which were recorded photographically.

### TESTS

Measurements of total and static pressures in the nacelle inlet and in the tail pipe, and of the total lift, drag, and pitching moment were made at a constant Reynolds number of 2,000,000 for Mach numbers from

0.18 to 0.92. The angle of attack was varied from  $-8^\circ$  to  $16^\circ$  at a Mach number of 0.18 and from  $-4^\circ$  to the highest angle obtainable at higher Mach numbers, the range being limited by model strength and tunnel power. Surface pressures were measured at selected Mach numbers near that for drag divergence. The model was tested with the air flowing through the nacelle and also with the air duct closed with the faired tail plug.

In order that the ram-recovery ratio of the inlet could be computed, the total pressures in the duct were measured with the rake installed 4 percent of the nacelle length behind the inlet. A rake of total- and static-pressure tubes installed in the tail pipe was used to measure the pressures required for the computation of the inlet-velocity ratio by the method of reference 5. The values of inlet-velocity ratio are based on the area of 8.12 square inches at the station of minimum nacelle-inlet area.

#### CORRECTIONS TO DATA

Tunnel-wall constriction effects on the Mach number and the dynamic pressure were evaluated by the method of reference 6. Although this method is intended to apply only to full-span models located centrally in the tunnel, it was used as a reasonable estimate of the constriction effects. The following table indicates the magnitude of the corrections applied to the Mach number and the dynamic pressure:

<u>Corrected Mach number</u>	<u>Uncorrected Mach number</u>	<u>Corrected <math>q_o</math> Uncorrected <math>q_o</math></u>
0.400	0.399	1.004
.700	.697	1.006
.800	.794	1.009
.850	.841	1.012
.900	.885	1.018
.920	.901	1.021

Corrections for tunnel-wall interference were evaluated by the method of reference 7, modified slightly to account for the sweep of the wing. The interference was taken into account by increasing the measured angle of attack an amount  $0.489 C_L$ , and by increasing the measured drag coefficient an amount  $0.0075 C_L^2$ . No correction was applied to the pitching-moment data.

A tare correction to the drag data, made necessary because of the flow over the exposed surface of the turntable, was measured with the model removed from the tunnel. The correction, in coefficient form, had a constant value of 0.0036, which was subtracted from the measured drag coefficient.

The internal drag due to flow through the nacelle was computed by the method discussed in reference 8, utilizing the total and static pressures measured with the rake in the tail pipe. The internal drag coefficient was subtracted from the measured drag coefficient corrected for tare drag and tunnel-wall interference to give the external drag coefficient. For moderate angles of attack, the internal drag coefficient varied from 0.0016 at a Mach number of 0.18 to 0.0006 at a Mach number of 0.92 and was affected only slightly by changes in the angle of attack.

## RESULTS AND DISCUSSION

### General

As noted previously, the model was tested with and without flow through the nacelle. For the condition with flow, the inlet-velocity ratio varied with Mach number and angle of attack as shown in figure 4. This flow condition is designated as  $V_1/V_0 = 0.9$  to 0.6 in figures 5 to 15.

### Force and Moment Characteristics

The lift, drag, and pitching-moment characteristics of the wing-nacelle combination with flow through the nacelle are presented in figure 5. Also shown in this figure are the data for the wing alone from reference 3. Figure 5(c) includes, in addition, the drag data for the wing-nacelle combination with no flow through the nacelle. The variation with Mach number of the aerodynamic characteristics of the wing-nacelle combination are presented in figures 6, 7, 8, and 9. The variation with lift coefficient of the drag-divergence Mach number of the wing-nacelle combination is shown in figure 10. In figures 11 and 12 are shown the variations with Mach number of the maximum lift-to-drag ratio, the lift coefficient for maximum lift-to-drag ratio, and the minimum drag coefficient.

From an examination of figures 5 and 7, it is evident that there was little change in the lift characteristics of the wing due to the addition of the nacelle. The pitching-moment data reveal that the addition of the nacelle resulted in a slight rearward shift of the aerodynamic center at zero lift, and in more positive values of the pitching moment for zero lift at all Mach numbers.

The variation with Mach number of the drag coefficient of the wing-nacelle combination for several lift coefficients is presented in

figure 8. In figure 8(b) it may be seen that, with no flow through the nacelle, the drag coefficient was generally greater than that with flow, the greatest increase occurring at negative values of the lift coefficient.

The variation with Mach number of the incremental drag coefficient is presented in figure 9. The incremental drag coefficient is defined as the increase in the external drag coefficient due to the addition of the nacelle. It may be observed that, prior to drag divergence, the incremental drag coefficient increased a greater amount at lift coefficients of  $-0.2$  and  $0$  than at lift coefficients of  $0.2$  and  $0.4$ . In figure 10, it may be noted that the drag-divergence Mach numbers of the wing-nacelle combination in the range of lift coefficients from  $-0.1$  to  $0.4$  were only about  $0.01$  or less lower in value than those of the wing alone. Moreover, the reduction of internal flow through the nacelle to zero apparently had a beneficial effect on the drag-divergence Mach numbers for lift coefficients from  $-0.1$  to  $0.4$ .

A method was indicated in reference 2 in which the effect of the nacelle on the drag-divergence Mach number of the wing could be estimated from low-speed data. The method was based upon the comparison of predicted critical Mach numbers of the wing and wing-nacelle combination at the crest points of various spanwise stations. The crest point is defined as the point at which the surface is tangent to the direction of the free stream. It was concluded in reference 2 that for the wing-nacelle combination of the present report no reduction of the drag-divergence Mach number would result from the addition of the nacelle, and that varying the inlet-velocity ratio would have little effect on the drag-divergence Mach number. These conclusions are substantially in agreement with the results of the present test.

In figure 11, the variations with Mach number of the maximum lift-to-drag ratio and the lift coefficient for maximum lift-to-drag ratio are compared with similar data for the wing alone. The reduction of the maximum lift-to-drag ratio due to the addition of the nacelle amounted to approximately 33 percent at a Mach number of  $0.18$ , but was smaller at the higher Mach numbers. Below the Mach number of drag divergence, the minimum drag of the wing was increased between 50 and 90 percent due to the addition of the nacelle.

#### External Pressure Distribution

The pressure changes at high subsonic speeds caused by the addition of the nacelle to the wing are illustrated by the diagrams showing lines of constant pressure coefficient, or isobars, presented in figure 13. Data for the wing alone and for the wing-nacelle combination with and without air flow through the nacelle are shown for angles

of attack of  $0^\circ$  and  $4^\circ$  at Mach numbers just below those for drag divergence. In order to provide a reference line from which to gauge the differences in the pressure distribution for the three configurations, the crest line, defined as the locus of crest points on the wing, is indicated on the isobar diagrams. The crest line has the added significance of being the dividing line between the positive and negative contributions of surface pressures to the pressure drag of the wing.

Figure 13(a) shows that for an angle of attack of  $0^\circ$  the addition of the nacelle to the wing considerably distorted the isobars in the region of the nacelle. A comparison of the pressure coefficients on the upper surface indicates that the effect of the nacelle was to make the pressure coefficients less negative over the wing at the station of the nacelle center line while making them more negative over the outer semispan. On the lower surface, the pressure coefficients became more negative with the addition of the nacelle, particularly in the region of the nacelle junctures and of the lip of the nacelle inlet on the lower nacelle meridian. Reduction of the inlet-velocity ratio from 0.64 to 0 created a small area of large negative pressure coefficients over the forward portion of the lower inboard nacelle juncture, but otherwise had little effect on the pressures over either the upper or lower surface.

Figure 13(b) shows that at an angle of attack of  $4^\circ$  the pressure changes due to the addition of the nacelle were similar to those at an angle of attack of  $0^\circ$  with the exception that the pressure coefficients on the upper surface ahead of the nacelle became more negative. The pressure coefficients in the lower junctures were considerably less negative at this angle of attack than at an angle of attack of  $0^\circ$ . The reduction of inlet-velocity ratio from 0.68 to 0 caused the pressure coefficients to become more negative near the nacelle inlet on both the upper and the lower surfaces.

#### Inlet and Internal Flow Characteristics

The distribution of the static pressure coefficient at several positions inside the nacelle inlet is presented in figure 14. At a Mach number of 0.18, the most negative pressure coefficients were found to exist at the position nearest the wing root with separation apparently taking place at an angle of attack of  $12^\circ$ . The separated region appears to have extended over a large portion of the lip at an angle of attack of  $16^\circ$ . At higher Mach numbers it can be seen that the lowest pressures continued to exist at this inlet position nearest the wing root, although separation did not occur within the angle-of-attack range of the investigation.

In figure 15, the variation of the ram-recovery ratio with Mach number at a station 4 percent of the nacelle length behind the inlet is presented for angles of attack of  $0^\circ$ ,  $4^\circ$ , and  $8^\circ$ . The ram-recovery ratio increased from 0.97 at a Mach number of 0.18 to 0.99 at a Mach number of 0.92.

## CONCLUSIONS

Wind-tunnel tests at Mach numbers up to 0.92 have been conducted on a wing-nacelle combination at a constant Reynolds number of 2,000,000. The model consisted of a jet-engine nacelle mounted on the lower surface of a wing having the leading edge swept back  $37.25^\circ$ . The results of a comparison with similar data for the wing alone may be summarized as follows:

1. Addition of the nacelle to the wing had little effect on the lift and pitching-moment characteristics of the wing. The aerodynamic center at zero lift was moved slightly rearward and the pitching moment was increased positively at all Mach numbers.

2. Addition of the nacelle with internal flow reduced the drag-divergence Mach number approximately 0.01 or less for lift coefficients between -0.1 and 0.4. The reduction of inlet-velocity ratio to zero increased the drag at Mach numbers below that for drag divergence, but had little effect on the drag-divergence Mach number.

3. In the angle-of-attack range from  $0^\circ$  to  $4^\circ$ , the ram-recovery ratio at a station 4 percent of the nacelle length behind the nacelle inlet was found to increase from approximately 0.97 to 0.99 as the Mach number was increased from 0.18 to 0.92. The corresponding change in inlet-velocity ratio was from 0.9 to 0.6.

Ames Aeronautical Laboratory,  
National Advisory Committee for Aeronautics,  
Moffett Field, Calif.

## REFERENCES

1. Hanson, Frederick H., Jr., and Dannenberg, Robert E.: Effect of a Nacelle on the Low-Speed Aerodynamic Characteristics of a Swept-Back Wing. NACA RM A8E12, 1948.
2. Dannenberg, Robert E., and Blackaby, James R.: An Experimental Investigation of a Jet-Engine Nacelle in Several Positions on a  $37.25^\circ$  Swept-Back Wing. NACA RM A50A13, 1950.
3. Edwards, George G., and Boltz, Frederick W.: An Analysis of the Forces and Pressure Distribution on a Wing With the Leading Edge Swept Back  $37.25^\circ$ . NACA RM A9K01, 1950.

4. Boltz, Frederick W., and Beam, Benjamin H.: The Effects of Compressibility on the Pressures on a Body of Revolution and on the Aerodynamic Characteristics of a Wing-Nacelle Combination Consisting of the Body of Revolution Mounted on a Swept-Back Wing. NACA RM A50E09, 1950.
5. Smith, Norman F.: Numerical Evaluation of Mass-Flow Coefficient and Associated Parameters From Wake Survey Equations. NACA TN 1381, 1947.
6. Herriot, John G.: Blockage Corrections for Three-Dimensional-Flow Closed-Throat Wind Tunnels, With Consideration of the Effect of Compressibility. NACA RM A7B28, 1947.
7. Sivells, James C., and Deters, Owen J.: Jet-Boundary and Plan-Form Corrections for Partial-Span Models With Reflection Plane, End Plate, or No End Plate in a Closed Circular Wind Tunnel. NACA Rep. 843, 1946.
8. Baals, Donald D., and Mourhess, Mary J.: Numerical Evaluation of the Wake-Survey Equations for Subsonic Flow Including the Effect of Energy Addition. NACA ARR L5H27, 1945.

*Semispan area (wing alone) = 8.283 square feet*

*Aspect ratio (wing alone) = 6.04*

*Taper ratio = 0.50*

*$\bar{c}$  (wing alone) = 1.728 feet (parallel to root chord)*

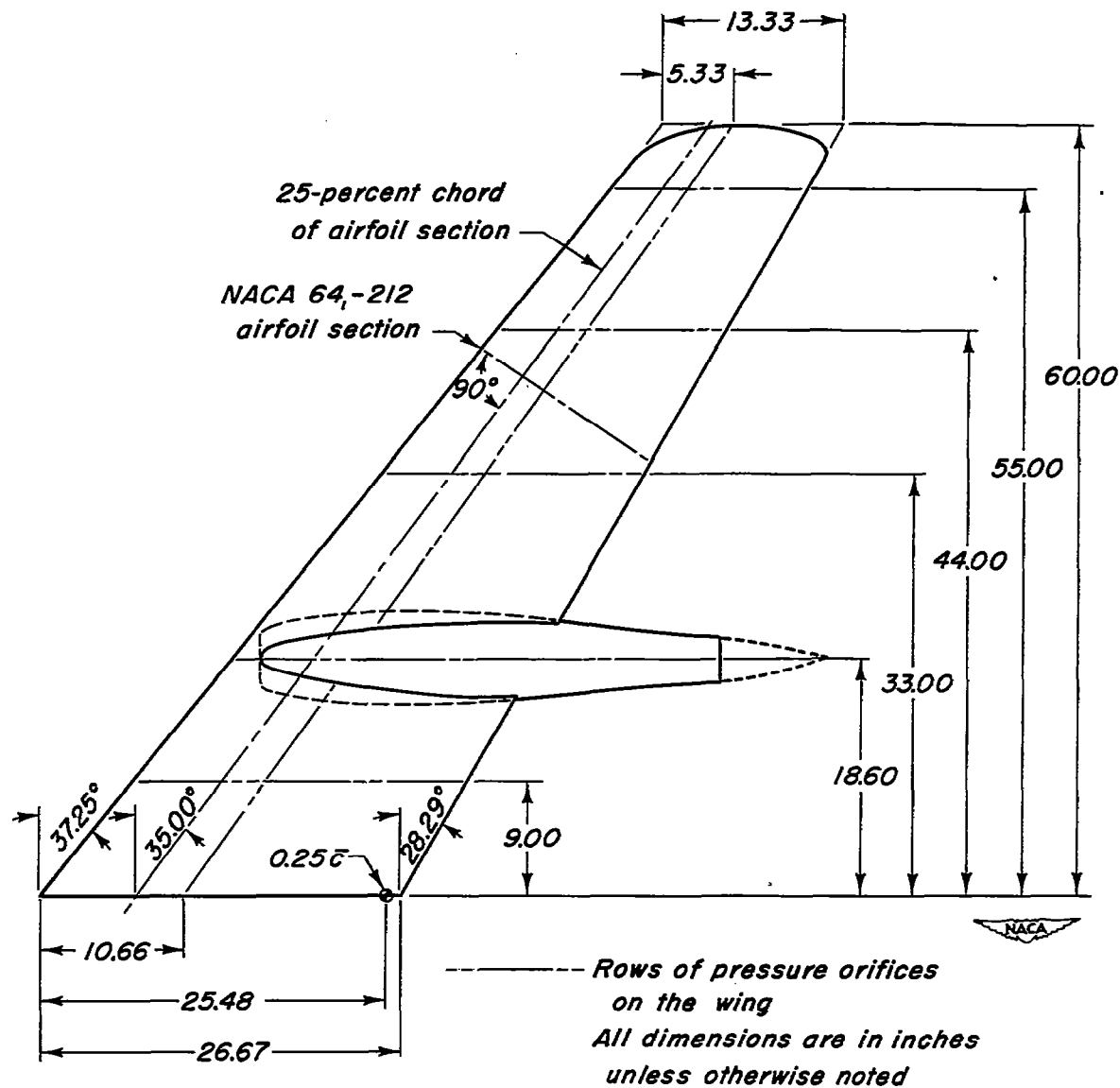
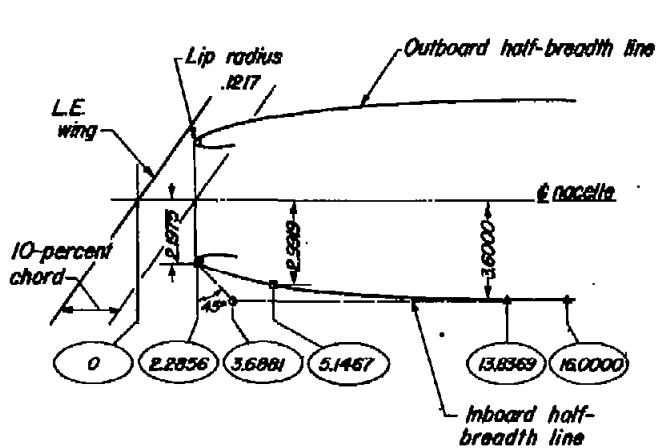


Figure 1.- A plan view of the upper surface of the wing-nacelle combination.



Note:

1. Upper forward body above wing is formed by radii with centers at nacelle center line on nacelle reference plane.
2. Inboard external lines forward of station 6.5 which lie between nacelle reference plane and wing lower surface are normal to nacelle reference plane and tangent to the half-breadth.
3. Outboard external lines forward of station 10.5 which lie between nacelle reference plane and wing lower surface are normal to nacelle reference plane and tangent to the half-breadth.
4. Afterbody (station 16 to 36) is circular.

5. Lower forebody (station 2.25 to 16) is symmetrical about vertical center plane.
6. Location of jet-unit entry is approximately station 7.5.
7. Control lines are straight between tangent points.
8. All dimensions are given in inches model scale.
9. Nacelle frontal area is 40.715 square inches.

Legend:

- ▲ Tangent point
- ◆ Intersection of tangent lines
- ▢ Shoulder point

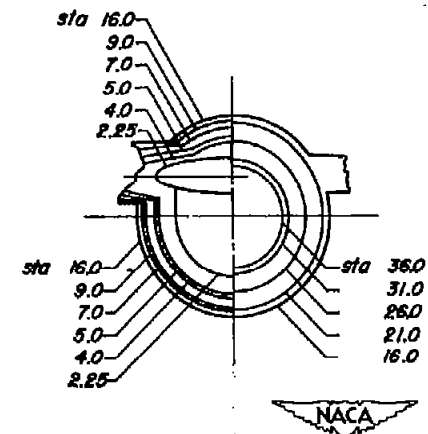
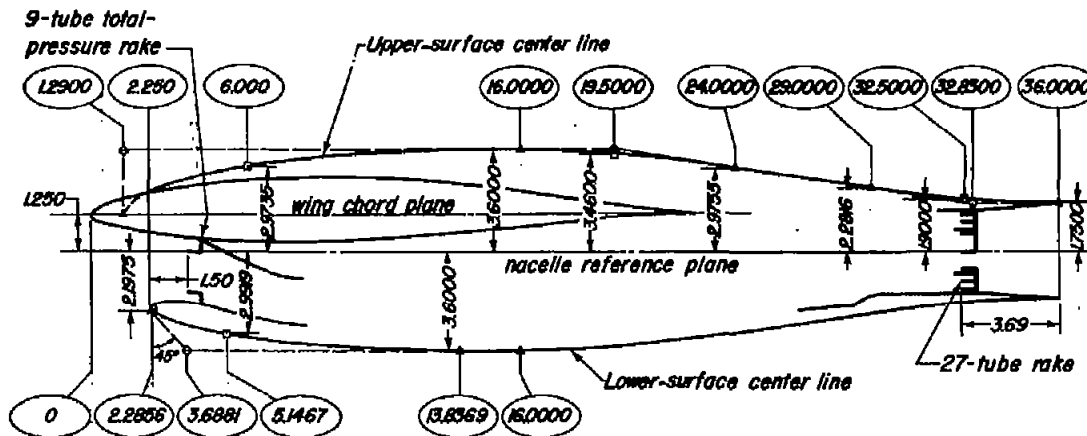


Figure 2.- The control lines of the nacelle (adapted from reference 2).



(a) Lower three-quarter front view.



(b) Upper three-quarter rear view.

Figure 3.— Model of the wing and nacelle mounted in the Ames 12-foot pressure wind tunnel.



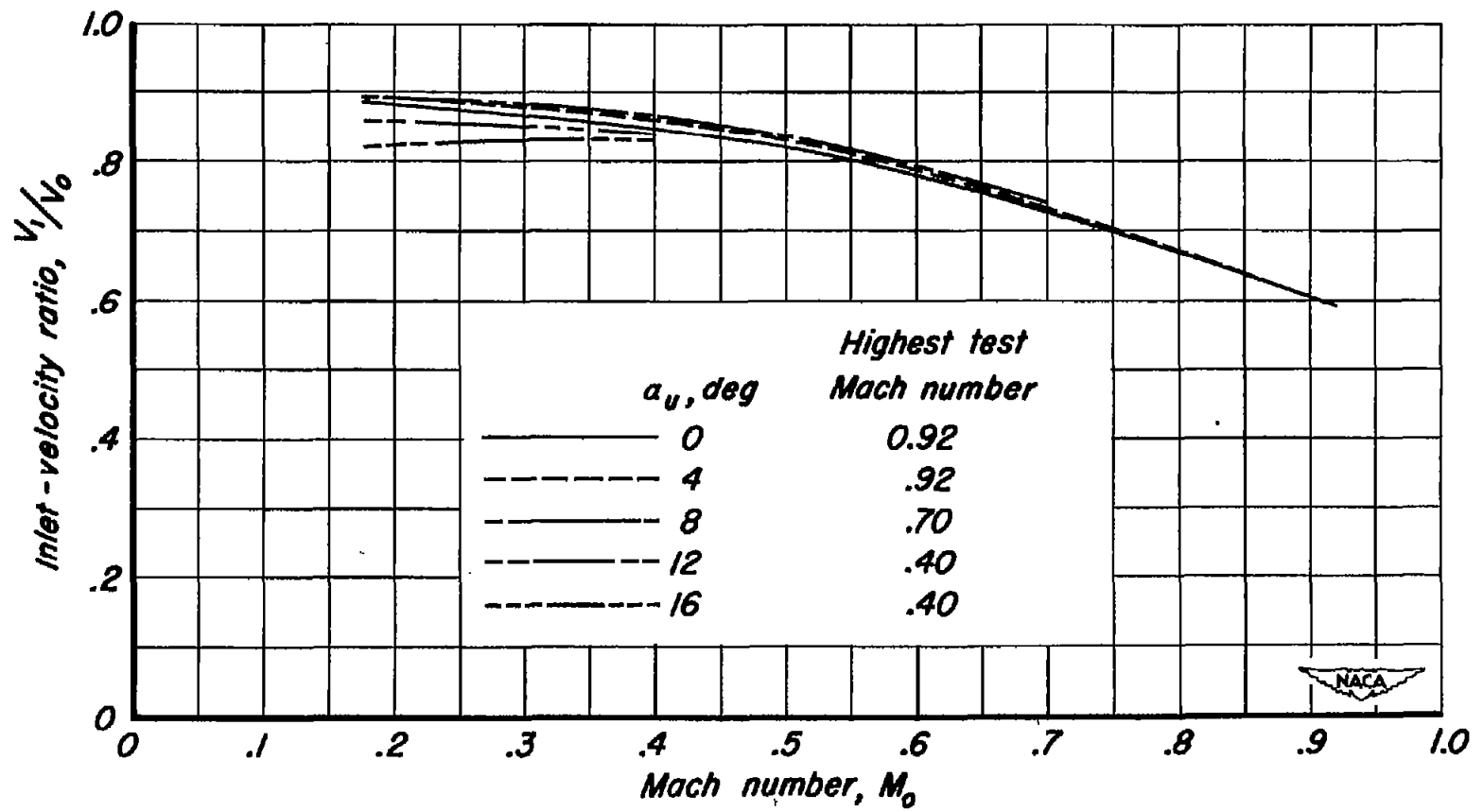
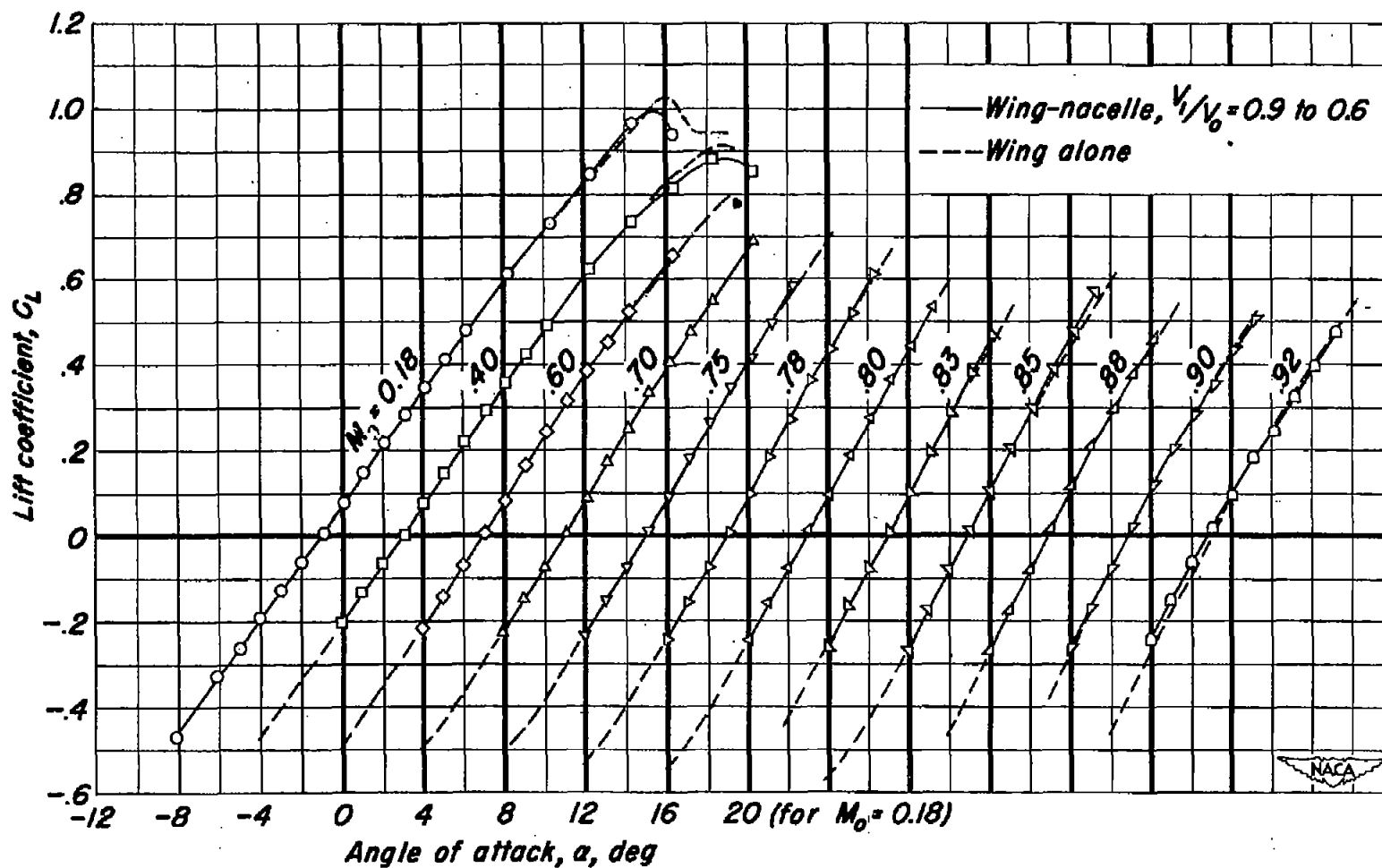
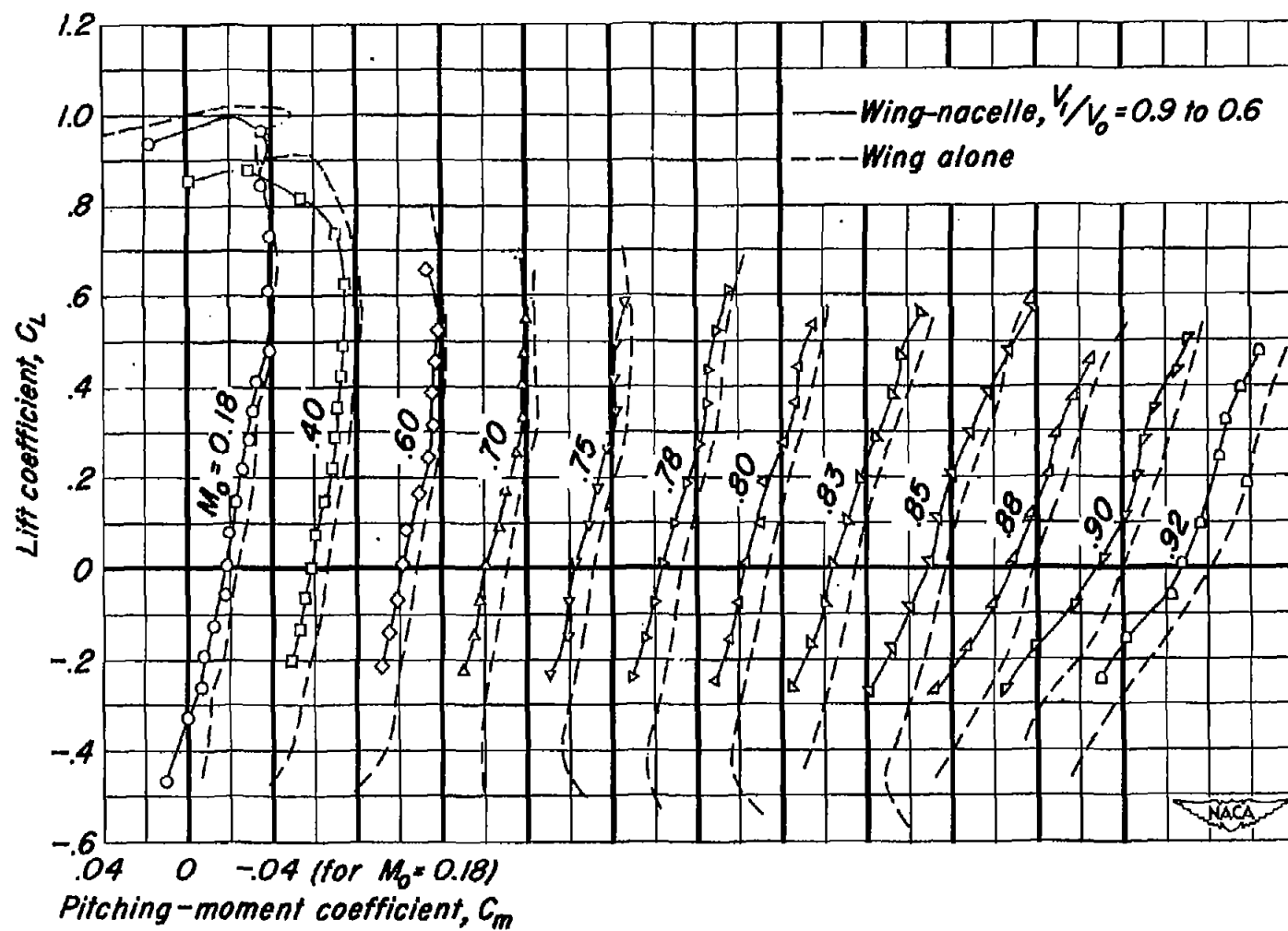


Figure 4.- The variation of the inlet-velocity ratio with Mach number.



(a)  $C_L$  vs  $\alpha$ .

Figure 5.-The aerodynamic characteristics of the wing-nacelle combination for various Mach numbers.



(b)  $C_L$  vs  $C_m$ .

Figure 5.- Continued.

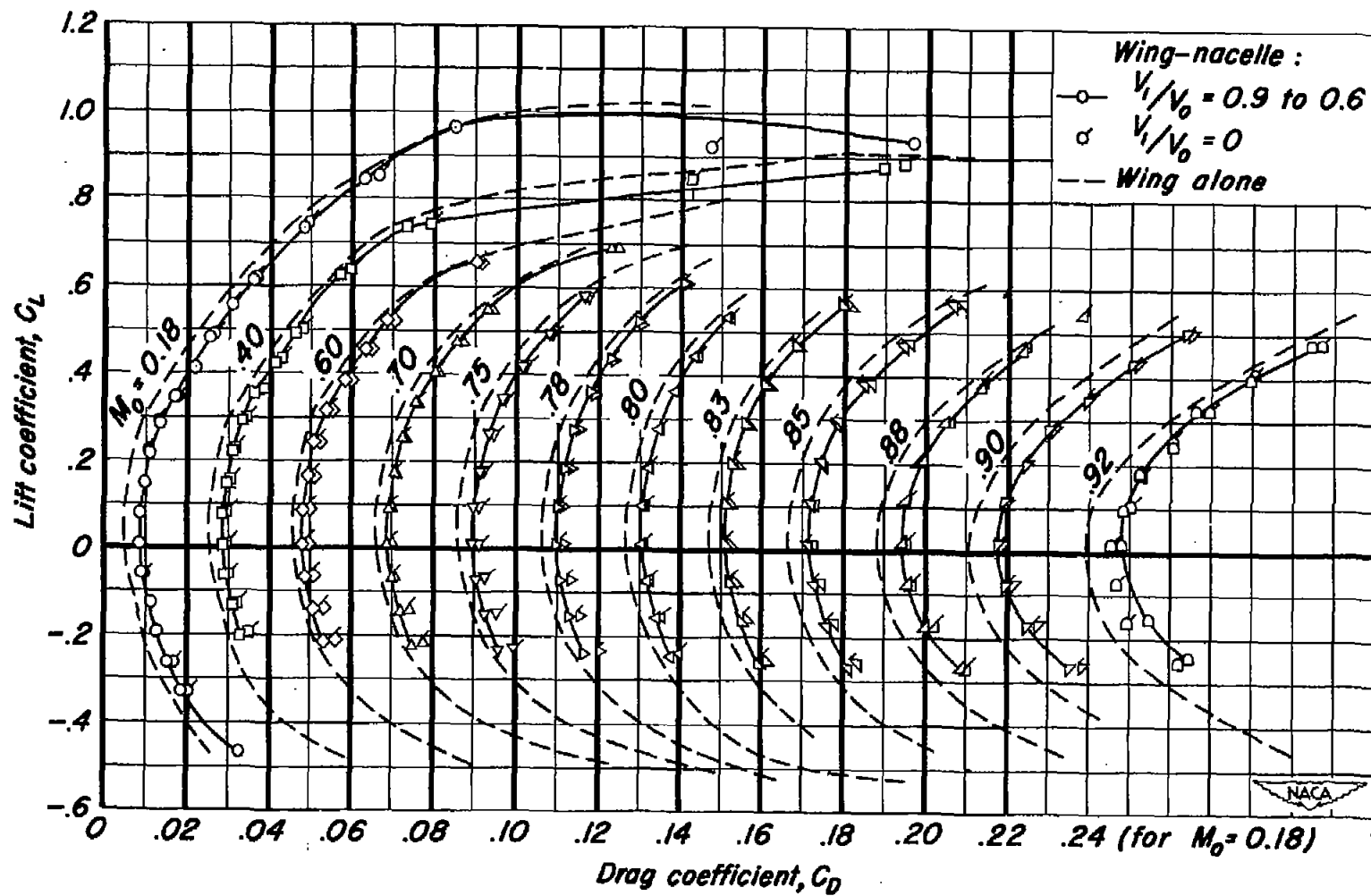
(c)  $C_L$  vs  $C_D$ .

Figure 5.- Concluded.

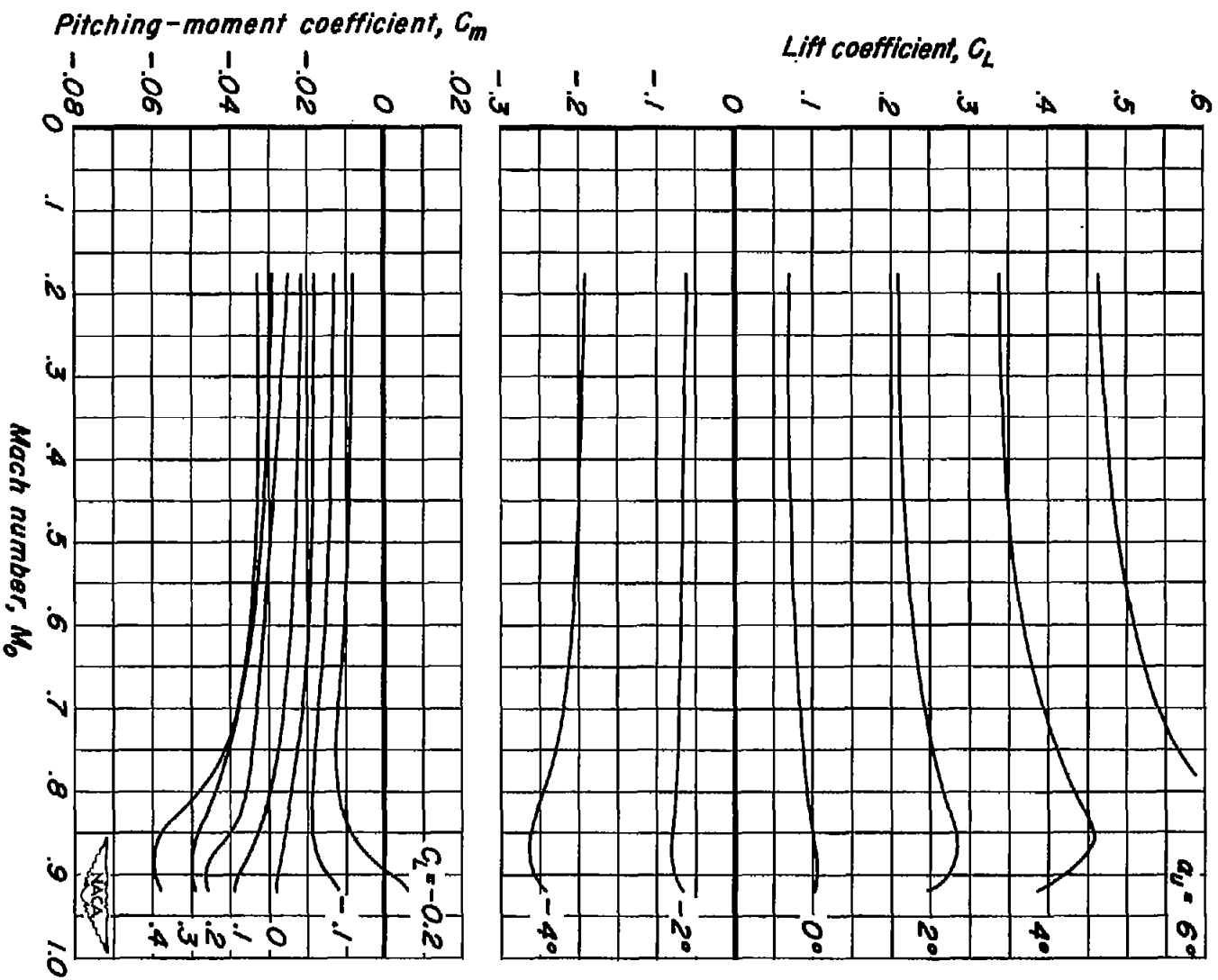


Figure 6.-The variation of the lift and pitching-moment coefficients with Mach number  $V/V_0$ , 0.9 to 0.6.

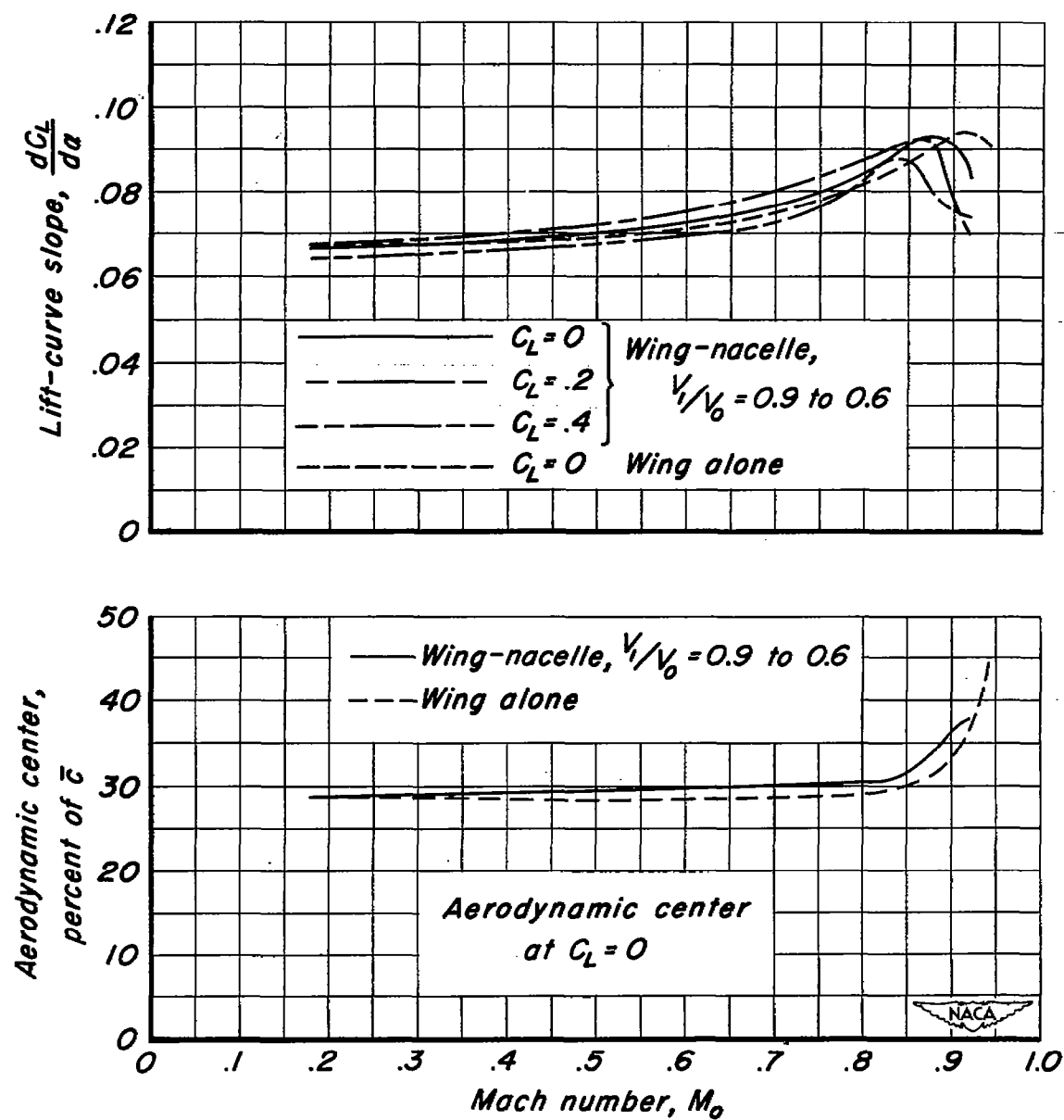
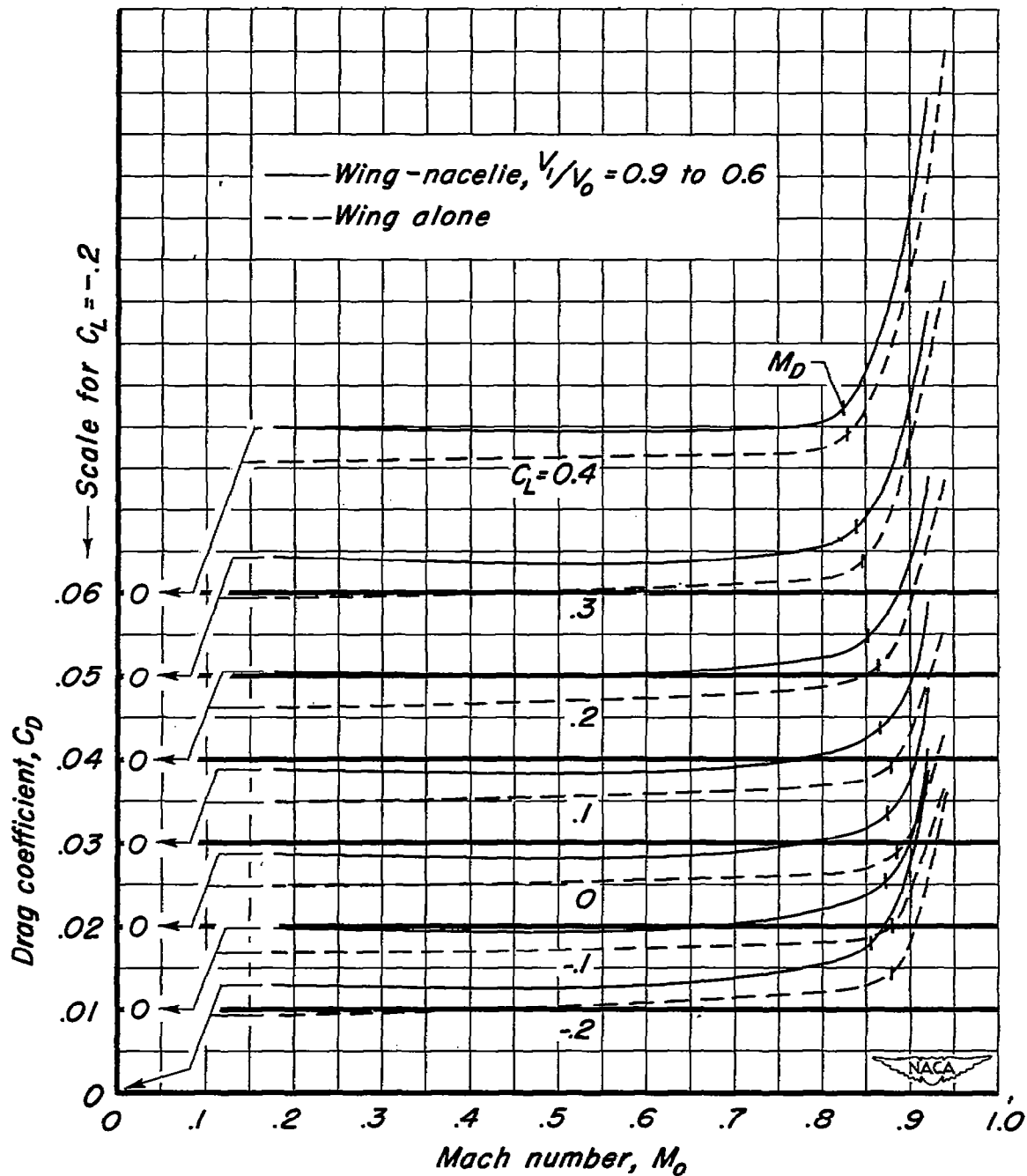
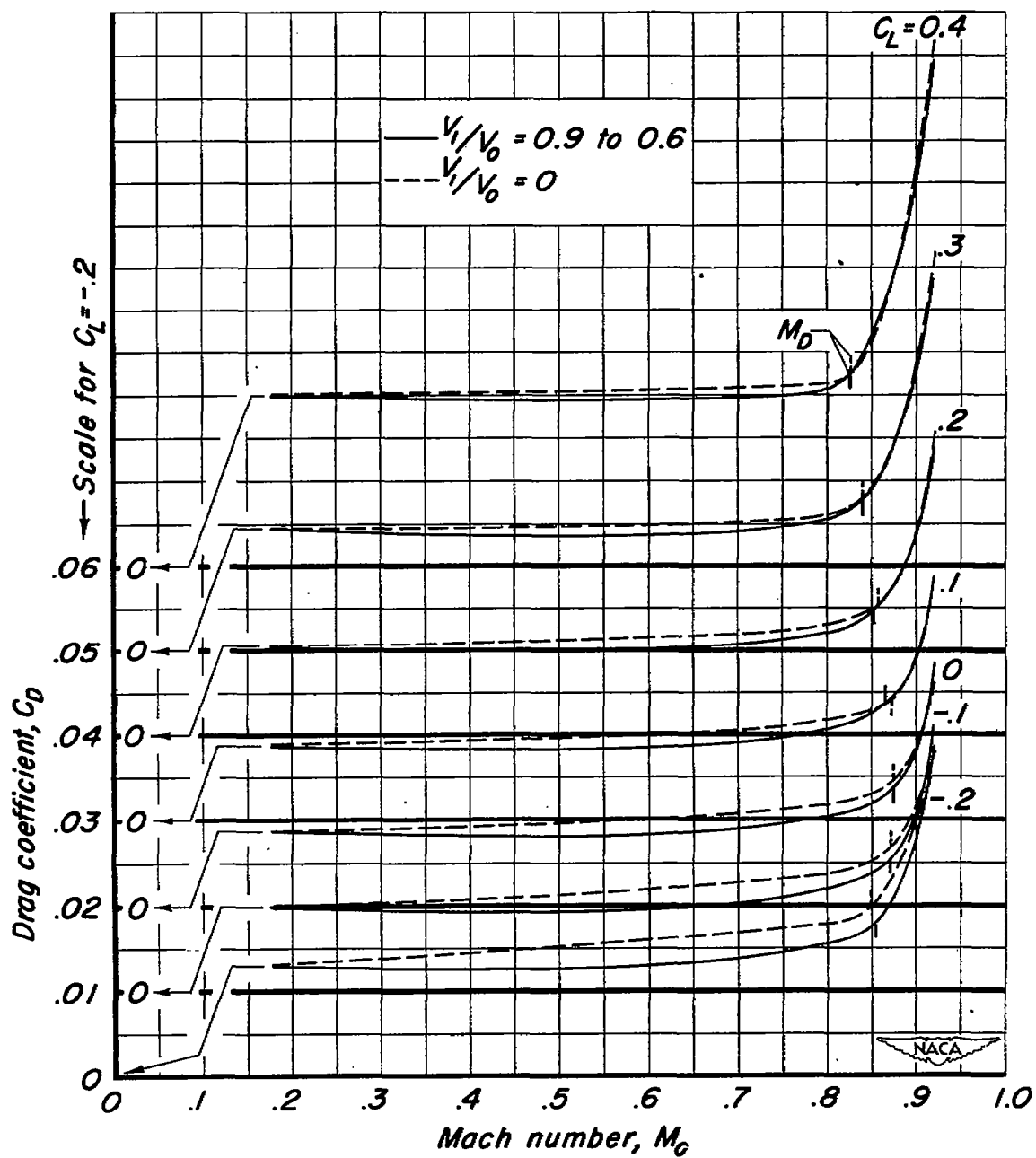


Figure 7.-The variation of the lift-curve slope and the location of the aerodynamic center with Mach number.



(a) Wing alone and wing-nacelle combination with internal air flow.

Figure 8.-The variation of the drag coefficient with Mach number.



(b) Wing-nacelle combination with internal air flow and without internal air flow.

Figure 8.- Concluded.

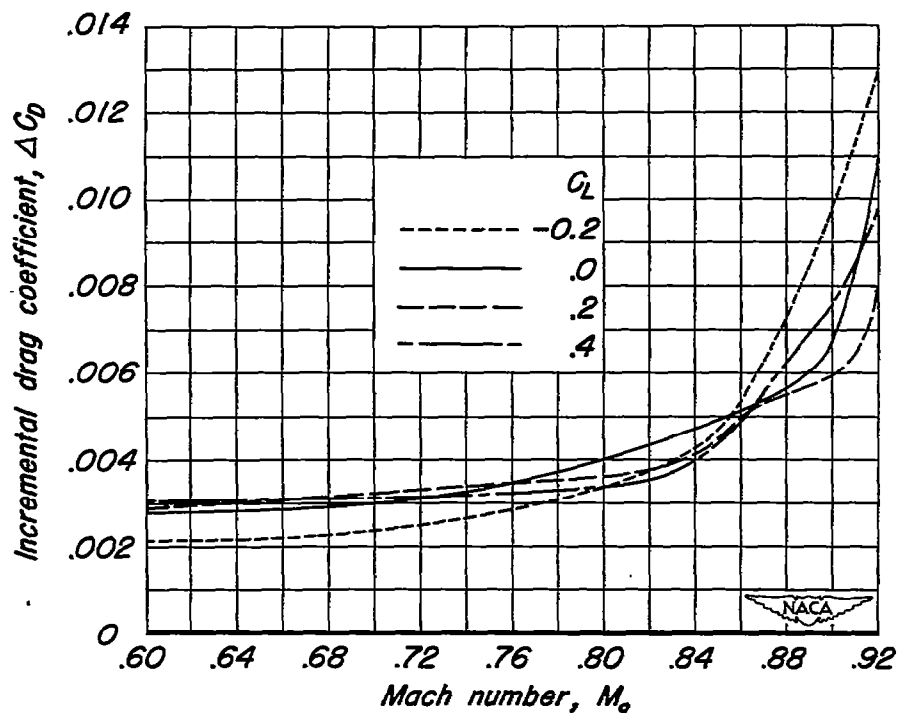


Figure 9.- The variation of the incremental drag coefficient with Mach number;  $V_i/V_0$ , 0.9 to 0.6

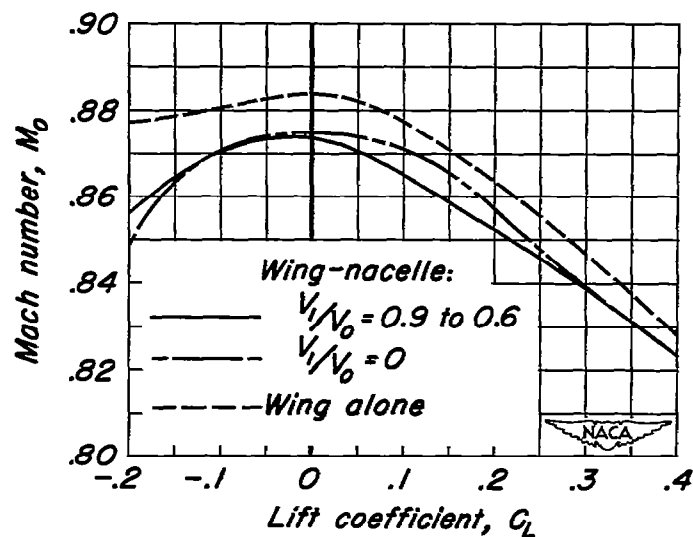


Figure 10.- The variation of the drag-divergence Mach number with lift coefficient.

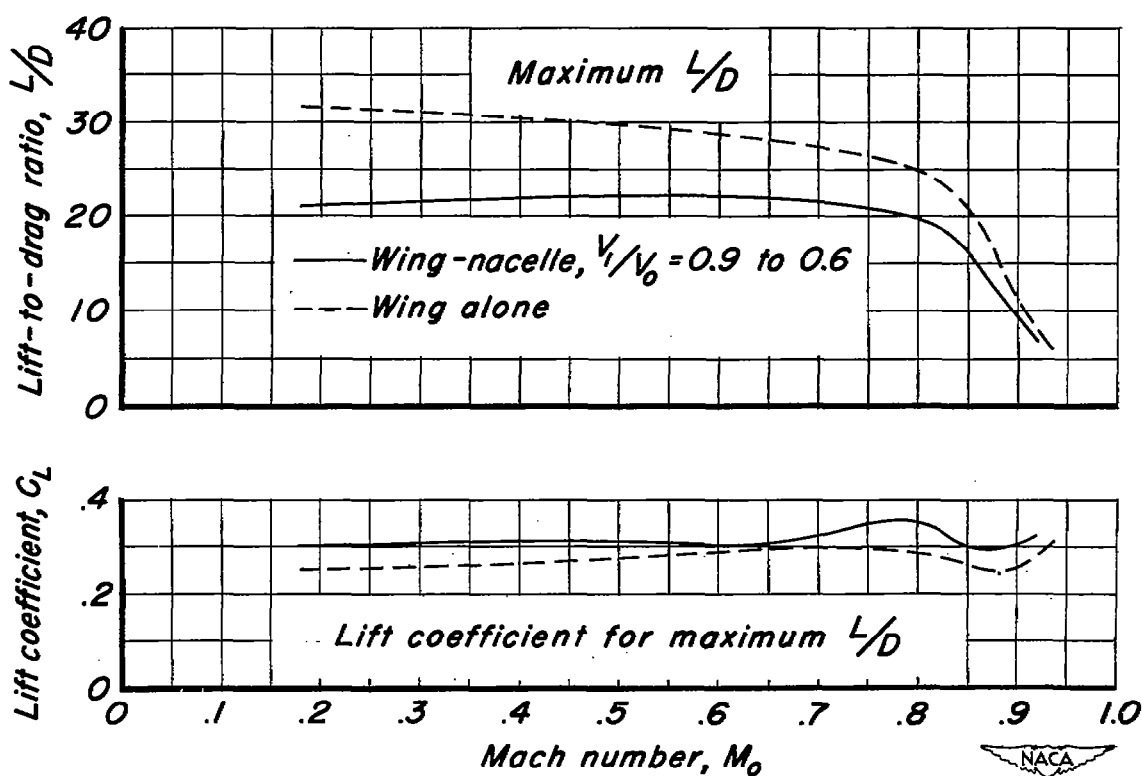


Figure 11.- The variation of the maximum lift-to-drag ratio and the lift coefficient for the maximum lift-to-drag ratio with Mach number.

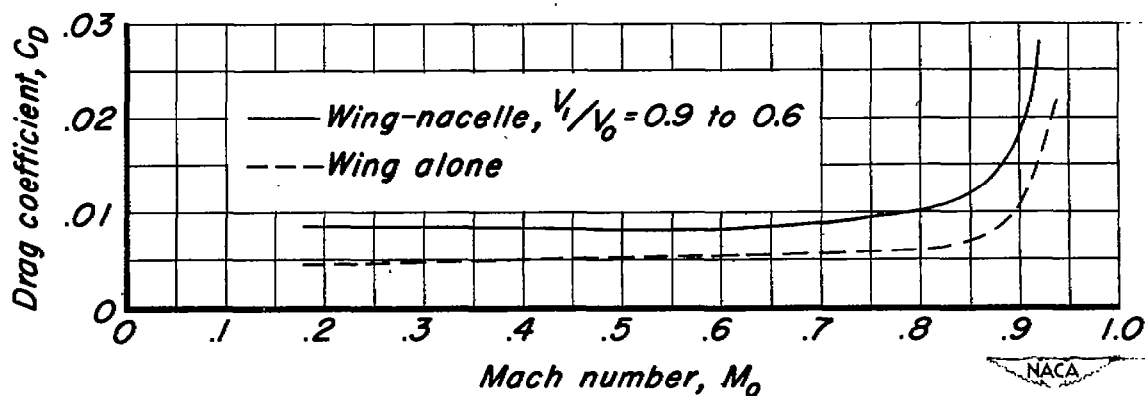


Figure 12.- The variation of the minimum drag coefficient with Mach number.

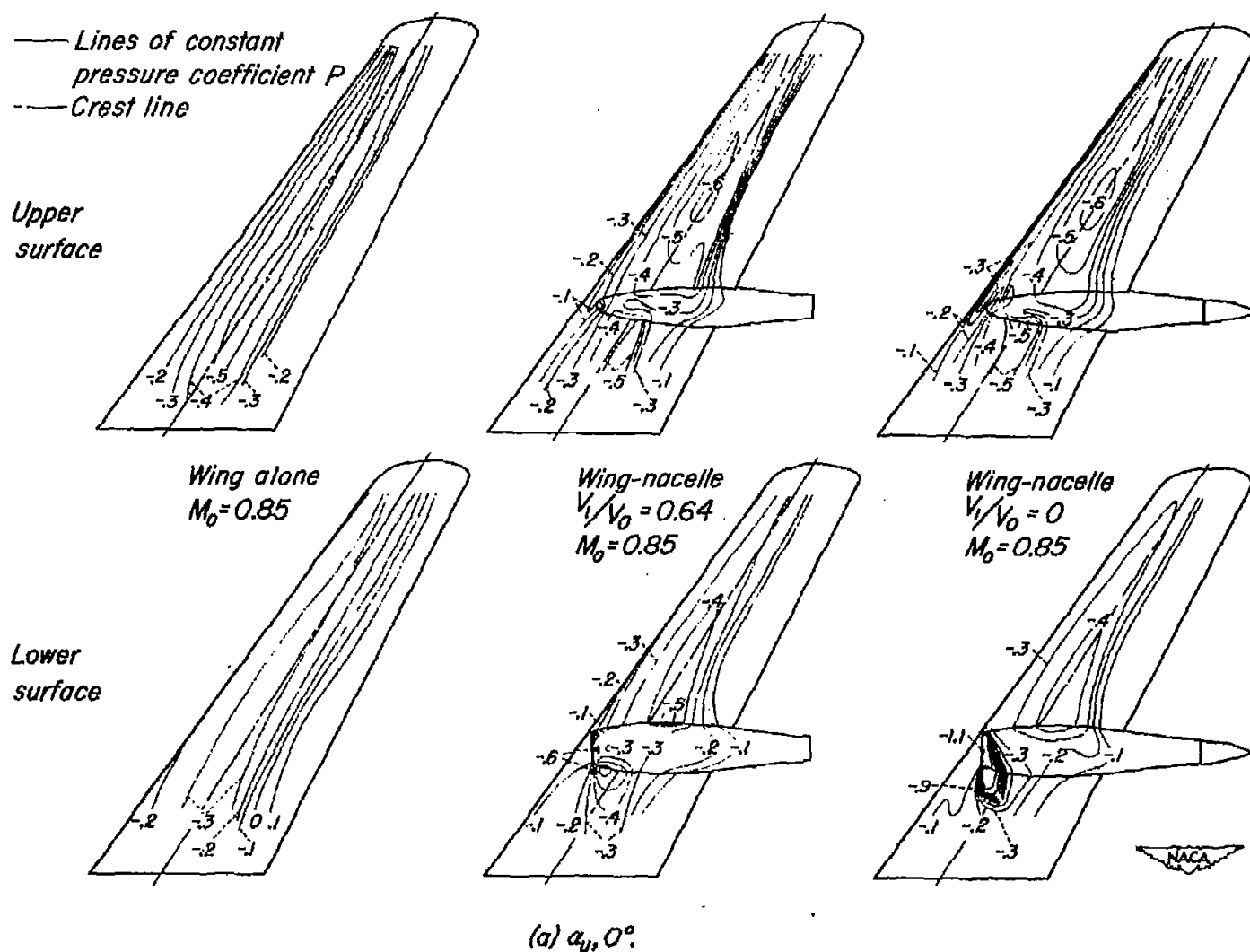


Figure 13.—The lines of constant pressure coefficient on the wing alone and on the wing-nacelle combination.

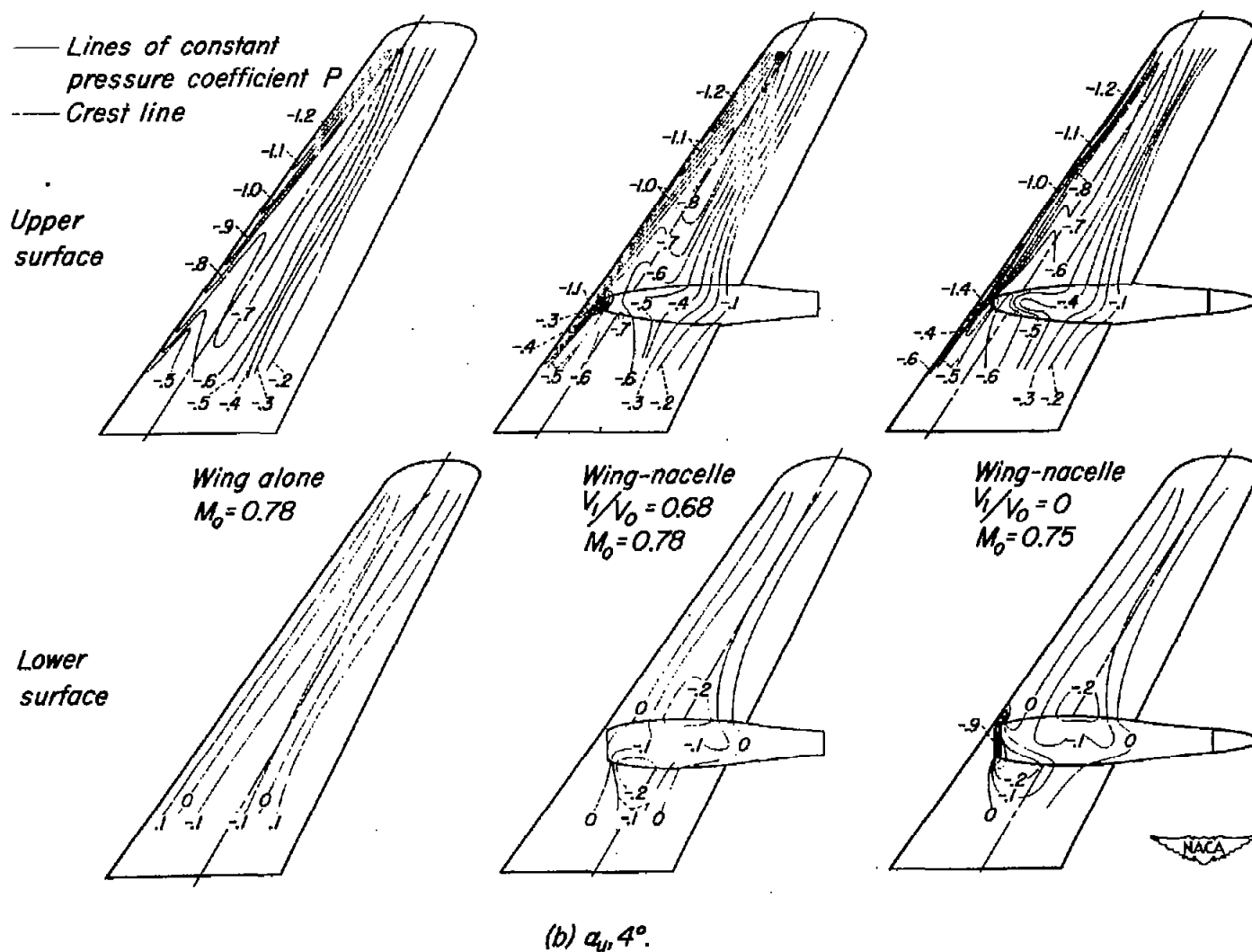


Figure 13.- Concluded.

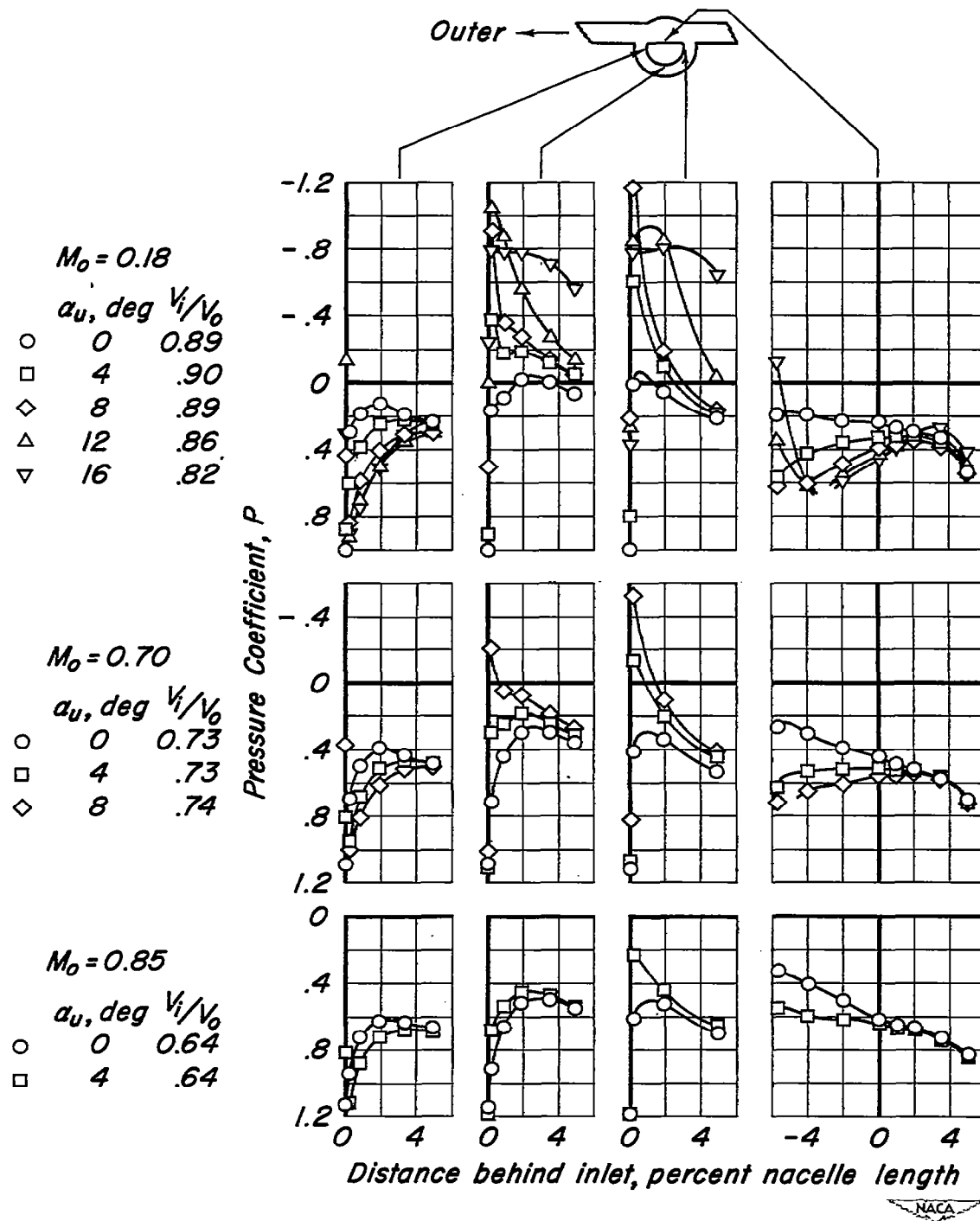
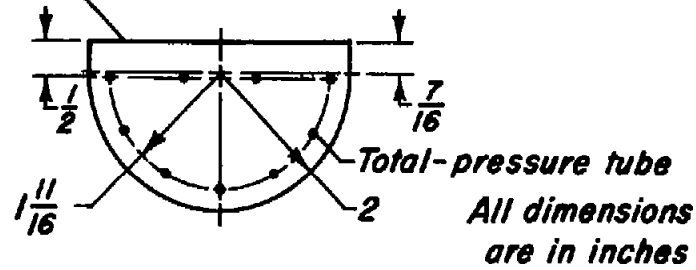


Figure 14.—The distribution of pressure coefficient inside the lip of the nacelle inlet at various Mach numbers.

Sectional view of the nacelle air duct at a plane through the forward end of the tubes



Tube locations of the rake used to measure ram recovery

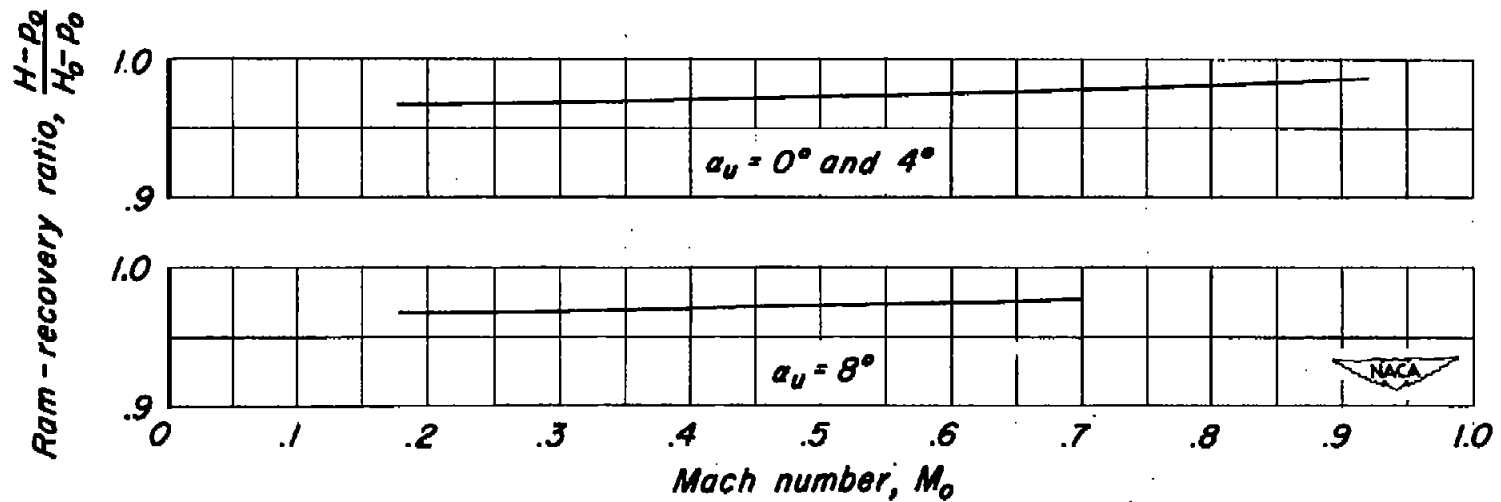


Figure 15.-The details of the inlet rake, and the variation of the ram-recovery ratio with Mach number at a station 4 percent of the nacelle length behind the inlet;  $V_1/V_0$ , 0.9 to 0.6.

NASA Technical Library



3 1176 01425 9478